Milestone Report

Experimental measurement of the effective contact angle for solvent/packing interactions in a structured packed column for CO_2 capture

Work Performed Under
Activity Number 0004000.6.600.007.002 ARRA

Prepared by
Pacific Northwest National Laboratory
Richland, Washington 99352

Prepared for the
U.S. Department of Energy
National Energy Technology Laboratory

October 2023

Revision Log

Revision	Date	Revised By:	Description
1.0	10/23/2023	Rajesh Singh	1st draft
1.1	10/26/2023	Susan Ennor	Technical Editing
1.2	10/28/2023	Rajesh Singh	2nd Draft
1.3	10/30/2023	Jennifer Yao	3rd edit
1.4	10/31/2023	Yucheng Fu	Figure Modification
1.5	10/31/2023	Rajesh Singh	4th Edit
1.6	10/31/2023	Zhijie Xu	Editing

Disclaimer

Acknowledgment of Funding

This project was funded under the Carbon Capture Simulation for Industry Impact ($CCSI^2$) under the following FWPs and contracts:

PNNL–68494

Contents

List of Figures

List of Tables

Executive Summary

The contact angle is a critical factor for determining the effective mass transfer area for carbon dioxide (CO_2) capture via the chemical absorption process in a packed column, and thus the overall capture efficiency of the packed column. Many widely used commercial packings involve microscale features (perforation, corrugation, etc.) that may also affect the wetting behavior. This study proposes a systematic method of using a modified Wilhelmy plate to measure the effective contact angle to characterize the solvent and featured packing interaction. In lieu of computational efforts relying on assumptions guided by semi-informed correlation, the proposed method directly measures the effective contact angle as a function of the solvent and packing thermophysical and hydrodynamic properties. The characterization of the effective contact angle is then integrated in the computational fluid dynamics modeling to reduce uncertainty in the prediction of effective mas transfer area. Experiments were conducted for stainless steel coupons using water and aqueous sodium hydroxide (NaOH) solvent for verification of the proposed experimental protocol. The surface tension of the aqueous NaOH solvent was altered using surfactant and antifoam. The effective contact angle increases with the increased value of the surface tension for flat stainless steel sheets. On the other hand, effective contact angles do not vary in Mellapak coupons for aqueous monoethanolamine (MEA) and NaOH solvent. In this case, surface textures and design of packing unit play a dominant role in the contact angle of solvents. Furthermore, CO_2 loading has a significant effect on the contact angle for Mellapak coupons. As expected, the contact angle decreases with the increasing temperature of CO_2 capture solvents (MEA, EEMPA). The effective contact angle measurement using the Wilhelmy plate method can provide more accurate and efficient solvents for characterizing the solvent-packing surface interactions. Subsequently, the present method enhances the accuracy of the prediction of the effective mass transfer area in carbon capture by solvent absorption.

1.0 Introduction

Carbon dioxide (CO_2) emissions from the combustion of fossil fuels, especially from coal and natural gas power plants, are still the main source of anthropogenic greenhouse gases causing global climate change [1, 2]. Efforts have grown unprecedentedly to demonstrate the techno-economic viability of technologies used to capture CO_2 from power plant flue gas streams [3]. Capturing CO_2 requires a lot of energy; therefore, the focus of each individual technology is to reduce the associated energy costs whenever possible. Among the various technologies, the solvent-based carbon capture system (CCS) is probably the prospective technology to be deployed in power plants [4]. The performance of solvent-based CCS, especially in absorbed packed column designs, is highly dependent on the interaction between the solvent and the selected packing [4-8]. Having relevant information is critical to achieve CO_2 capture in both coal and natural gas using aqueous and water-lean solvents. However, due to the complexity of the technology, the current absorption column design is mostly based on empirical correlation. Packed columns are designed based on semi-empirical correlations for estimating pressure drop across column, mass transfer coefficients, and effective mass transfer area. Correlations are based on the measurement of various parameters (e.g., solvent viscosity, contact angle, surface tension, etc.) to predict the effective mass transfer region, which affects the overall performance of the packed column [5-7, 9-15]. Recent studies [11, 12, 16, 17] have shown that contact angle is the critical parameter for dictating wetting of packed column, thereby effective mass transfer area. Accordingly, accurate estimation of the effective contact area is important for predicting the effective mass transfer area in a packed column.

Wetting of columns is strongly connected to the packing surface behavior [18], i.e., contact angle, surface texture, and sheet design. The contact angle is a property of solid-liquid systems in a given environment [19] and a solvent can have different values of contact angle depending on the solid surface. A smaller contact angle value increases wetting, which improves the effective mass transfer area [9, 11]. In addition, surface texture or embossing promotes wetting of the packed column [8, 20] by reducing the value

of the apparent contact angle [21, 22]. Recent studies of a rivulet falling over an inclined plate [11] and a single corrugated sheet [12] have shown that the effect of contact angle on the surface area is related to the surface tension of the liquid. The influence of the contact angle on the interfacial area [9, 11, 12] was found to be strong for a solvent with a lower surface tension. Further, most empirical models of the interface area [8, 23] assume a uniformly distributed fully wetted plate in each packing section and neglect the effect of the contact angle. In contrast, Rocha et al. [14] and Gualito et al. [24] emphasize the effect of the contact angle in their model. They modified the model of Shi and Mersmann [9] by introducing a regulation parameter. Shi and Mersman [9] developed a model using a liquid falling on an inclined plate. Surface tension is a critical factor that governs the spreading of a liquid on a solid surface.

The determination of the contact angle is difficult because it depends on several factors, including packing type, surface roughness, solvents, temperature, etc. [25]. The two types of packing for the packed columns—structured packing and random packing—are often made from a variety of materials, including ceramics, metal, and polymers. Structured packings may have been mechanically processed (grooved, lanced, textured) and have surface features on a micro (0.1–-0.25 in.) or macro (0.5–2 in.) scale in the form of corrugation, bunches, and holes (Fig. 1). When measuring contact angle optically with sessile droplets, these surface textures scatter the data [5]. Therefore, it is essential to increase the precision of the contact angle measurement to forecast the performance of packed columns for CO_2 capture. Sebastia-Saez et al. [26] recently measured the contact angle between aqueous monoethanolamine (MEA) solvent and Mellapak sheet using the sessile drop method. However, they discovered nearly identical contact angle values on each side of the droplet. It is important to keep in mind that the contact angle changes during wetting and shows distinct values at the advancing and receding ends. This study suggests the Wilhelmy plate method for measuring contact angle, while considering the influence of the packing coupon surface characteristics and geometry, provide a more accurate representation of the wetting process. The new approach will track the wetting force profile and nominal contact line length along the coupon immersion direction into the solvent in comparison to the traditional Wilhelmy plate employing a rectangular flat plate. The effect of the packing

geometry and features on solvent wetting behavior and, ultimately, the capture efficiency of a CCS, can be considered in the computed effective contact angle.

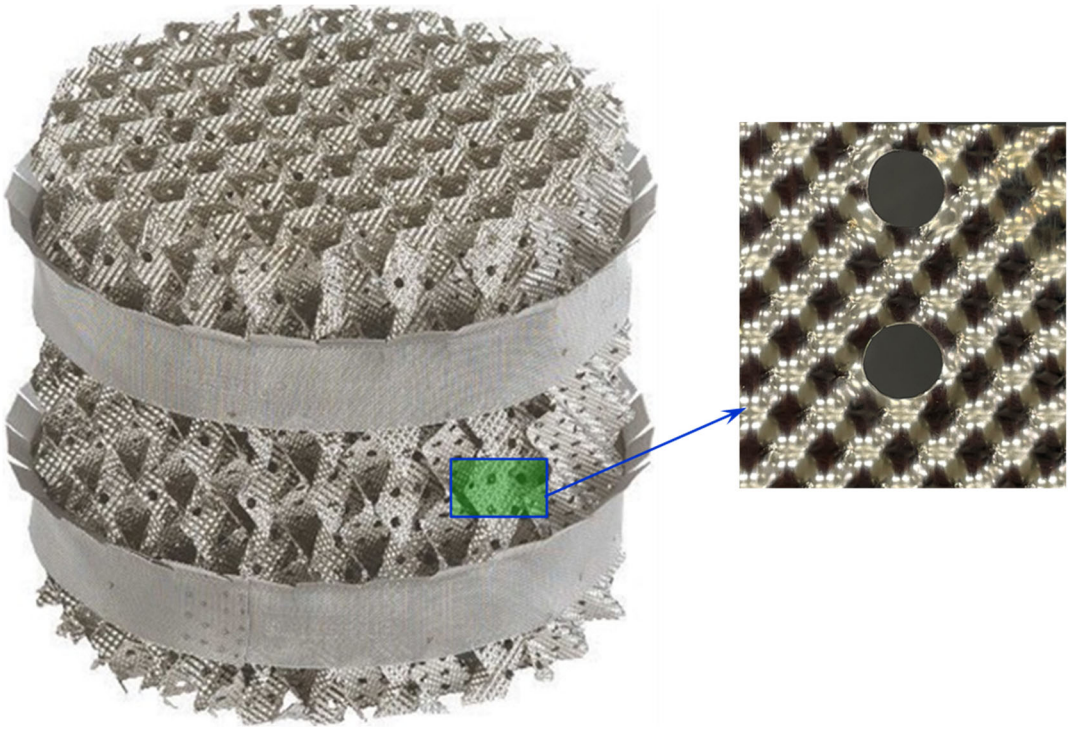

Fig. 1: Image of a packing unit showing the arrangement of corrugated sheets in a structured packed column (source: https://www.sulzer.com/en/shared/products/mellapak-and-mellapakplus). The exploded view shows the design of the corrugated sheet.

This report presents the measurement of effective contact angle on the corrugated sheet used in the packing units of various Mellapak structured packed columns using the modified Wilhelmy plate technique [27]. The promising single-component derivative N-(2-ethoxyethyl)-3-morpholinopropan-1-amine (EEMPA) of the CO_2-Binding Organic Liquid (CO_2BOL) developed at Pacific Northwest National Laboratory (PNNL) is used as the primary solvent, given its significant low operational heat and total costs for CO_2 capture [28, 29]. In addition, two aqueous solvents namely sodium hydroxide (NaOH) and MEA, a traditional solvent used in carbon capture, are examined with the Mellapak coupon for effective contact angle measurement. In addition, the effects of the CO_2 loading and temperature on the contact angle on Mellapak coupons also are examined.

2.0 Experimental Method and Materials

2.1 Wilhelmy plate method

The Wilhelmy plate technique [27], developed by Ludwig Wilhelmy, is used to measure surface tension and adhesion/cohesion for a particular surface and solvent pair using a tensiometer. This methodology relies on slowly immersing and retracting a coupon, whose weight is tracked via a microbalance, into and out of a solvent to allow wetting to occur and generate a wicked wetted surface. Subsequently, the Wilhelmy plate measurements allow for direct measurement of the surface tension and the dynamic contact angle. The Wilhelmy plate method is based on force balance, which involves balancing the interfacial tension force and gravity acting on a thin plate immersed vertically on the gas-liquid interface [28]. Coupon weight measured during the immersion allows for deconvolution of the wetted force and buoyancy force imparted during wetting that is correlated to the surface tension of the solvent, the contact angle during wetting and the wetted length/dimension. Fig. 2 depicts a perpendicularly submerged flat rectangular plate in liquid. Using this methodology, first a flat platinum plate surface with presumed zero contact angle and complete wetting can be immersed in the solvent to evaluate the surface tension of the solvent. The contact line perimeter of a rectangular plate (L) is calculated as $2\cdot(w+t)$, where w and t are the width and thickness of the plate, respectively. The surface tension force experienced by plate along the vertical direction $F_{\sigma,z}$ can be represented as:

$$F_{\sigma,z} = \sigma L \cos\theta\,, \tag{1}$$

where, σ is the surface tension of the solvent and θ is the contact angle between the liquid and solid substrate.

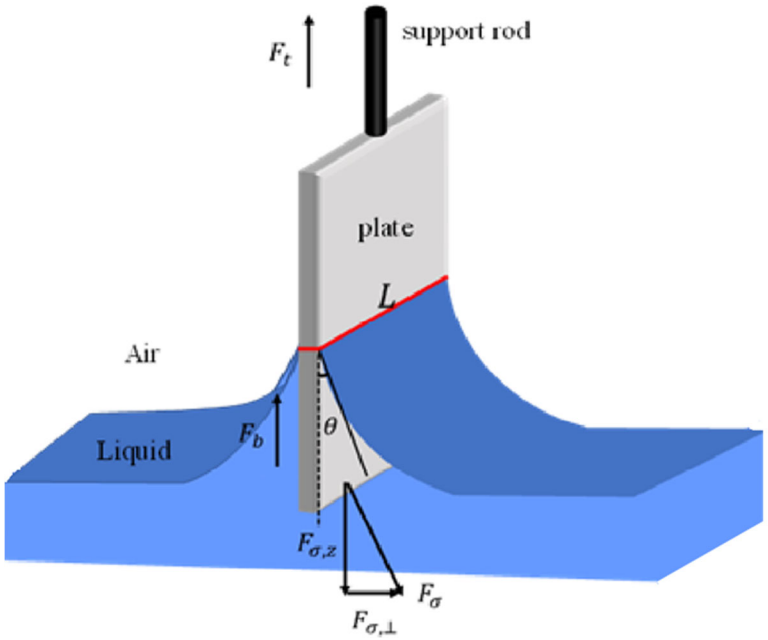

Fig. 2: Sketch depicting the working principle of the Wilhelmy plate method for contact angle (θ) and surface tension force ($\mathbf{F_\sigma}$) measurement.

2.2 Intersection method for contact angle calculation

As explained earlier, force tensiometer measures the weight (a representing of the vertical force) affecting to the balance when a coupon comes into contact with the solvent. The weight measurement was started at the coupon positioned 2 mm above the free surface of solvent. The tensiometer was tared to zero prior to the measurement. As seen in Fig. 3, the tensiometer displays the zero value of the force recorded to 0 - 2 mm along the coupon's depth. Once bottom of the coupon touches the free surface of the solvent, the tensiometer experiences sharp rise in the magnitude of the tensiometer force, and the maximum value of force is observed (~ 2 mm). As the coupon is submerged further, the tensiometer force progressively drops as the immersion depth varies (2 mm to 8 mm). The decrease in the magnitude of tensiometer force is due to increase of the buoyancy forces during immersion. The buoyancy force is computed from the displaced volume of the solvent that acts in upward direction. The variation of the tensiometer force along the coupon's immersion depth during the immersion stage is shown in Fig. 3. Note that the immersion of the coupon captures the advancing contact angle. Because of the irregular and complex surface features of the Mellapak coupon, the curve is not smooth, and peak and valley appear in the plot (Fig. 3). Conversely,

when a smooth, flat surface is submerged in a liquid, a smooth curve is seen, and the contact angle is represented from the tangent of curve. To overcome this, two separate lines were generated by connecting the peak and valley points of the curve. The tensiometer force was then determined by backward extrapolating these lines and intercepting them at the vertical line at a distance of 2 mm. The tensiometer force's highest ($\mathbf{F_{max}}$) and minimum ($\mathbf{F_{min}}$) values are shown by the intercepted points at the vertical axis. The average value of the tensiometer forces was used to calculate the effective contact angle, which was as follows:

$$\cos\theta_m = \frac{\left(F_{\min} + F_{\max}\right)}{2\sigma L} \tag{2}$$

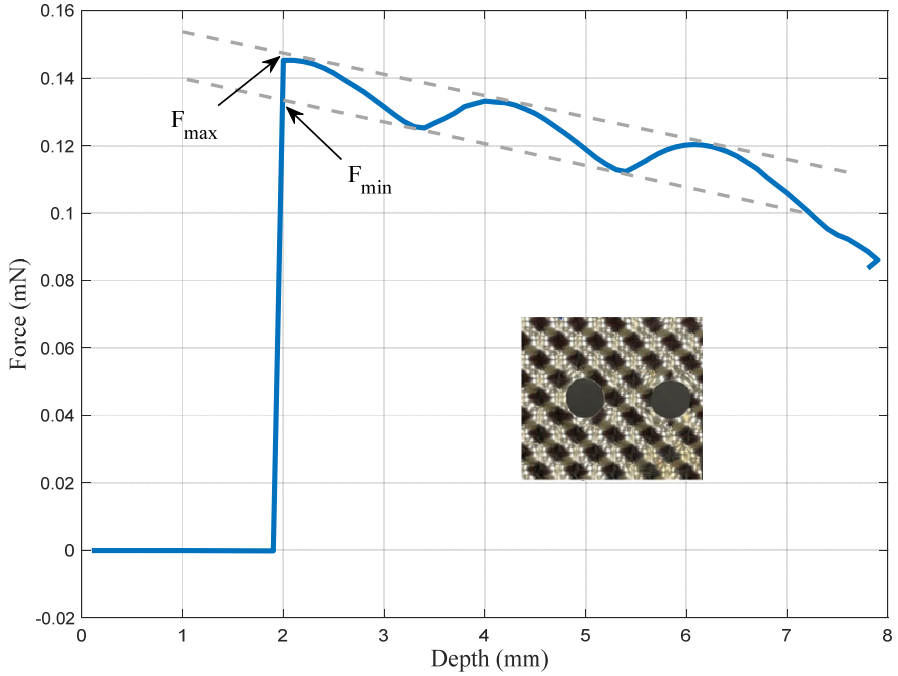

Fig. 3: Plot showing the variation of tensiometer force with depth of the Mellapak coupons immersed in the solvent. When the coupon is immersed in the solvent, the advancing contact angle is calculated. Inset shows the surface texture and embossment that causes the wavy nature of curve.

2.3 Coupon fabrication and surface characterization

The wetted perimeter and volume of the coupons are necessary for estimating the value of the effective contact angle. Mellapak and flat stainless-steel (SS) coupons (shown in Fig. 4(a&b)) were selected to represent the packing materials used in the structured packed columns and the SS sheet for verifications of

the Wilhelmy plate method by comparing the contact angle from open literature, respectively. Sheet stocks in 316 SS were purchased from packing manufacturer to prepare the packing coupons: the Mellapak is from Sulzer Chemtech, USA. Rectangular coupons with dimension of 2 cm x 2 cm were wire cut from the Mellapak sheet using electric discharge machining (EDM). For immersion and pulling of the coupon sample, a 4 cm 304 SS wire rod with a 1.145 mm diameter was spot welded to each coupon.

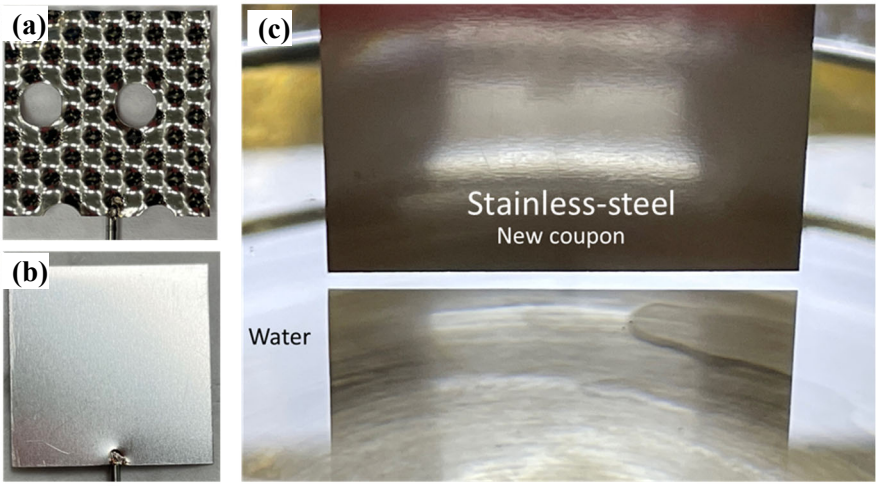

Fig. 4:Photographs depicting the working principle of the Wilhelmy plate method for contact angle (θ) and surface tension force ($\mathbf{F_\sigma}$) measurement. (a) Mellapak coupon, (b) stainless steel flat coupon, and (c) stainless steel flat coupon prior to immersion in water for measurements.

2.4 Image processing

The imaging of the coupon specimen was performed using the high-resolution ZEISS Versa 610 X-Ray microscope, which is capable of quick and nondestructive imaging with a spatial resolution of 500 nm (Fig. 5). Stacks of 2D slices of the scanned images were exported as DICOM (digital imaging and communications in medicine) image files for 3D geometry reconstruction. Using a customized in-house code created in MATLAB®, images were analyzed to extract the volume and wetting perimeter in the z-direction parallel to the attached rod. The computed tomography (CT) image, sliced in the x-y plane orientation, has an isotropic resolution of 0.02 mm/pixel. Each coupon sample is composed of 1018 two-dimensional slices, with each slice having a resolution of 1024 × 1024 pixels. The larger surface feature (> 0.10 mm) of coupons is fully resolved by X-ray CT (XCT) without losing any of the geometry's finer details.

In addition to XCT scanning, an optional microscope (Keyence) equipped with a 3D Optical Profiler was employed to capture images of the coupon, including its perimeter at a specific z-position (Fig. 5).

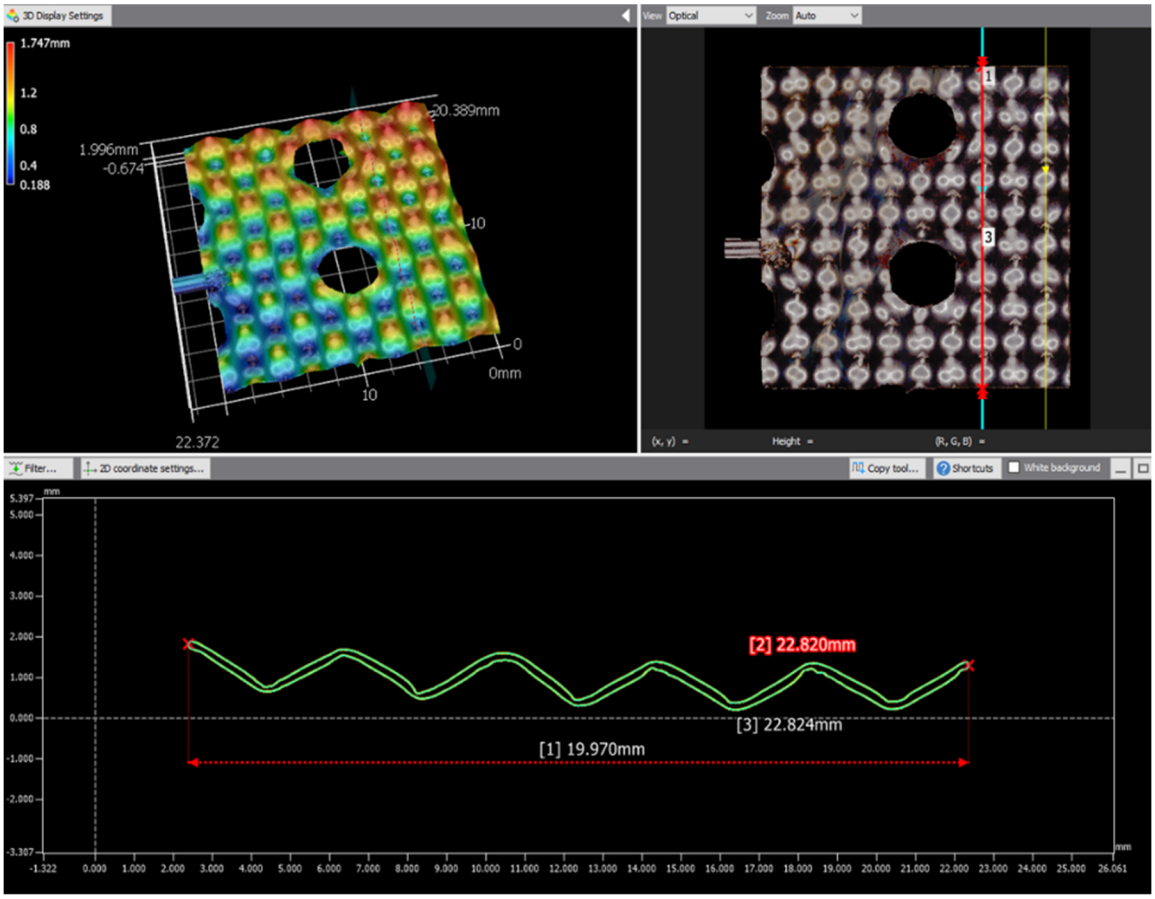

Fig. 5: Scanned image of the Mellapak coupon (top left). The bottom photograph shows the perimeter at a specific z-position indicated by the red line in top right image.

Details of the image reconstruction from the XCT image to the final computer-aided design (CAD) model has been extensively explained in a previous report [30]. Here, it is briefly described for readers understanding. The geometry of the Mellapak coupon was reconstructed and is depicted in Fig. 6. The coupon has a nominal height of 20 mm and a width of 20 mm. A SS rod has been welded at the top of the coupon to facilitate the conducted dynamic contact angle measurements. The perimeter profile along the z-direction can be obtained using the reconstructed 3D geometry. The normal of the coupon surface

undergoes a more significant directional change in the vicinity of the hole surfaces. The average coupon perimeter is approximately 45.13 mm, and the width of the coupon is approximately 22.41 mm.

As shown in Fig. 6, the Mellapak coupon exhibits a corrugated shape with periodic dents along the ridges. Two circular holes, each with a diameter of 4 mm, are situated in the center of the coupon. In the packed column, the holes on the packing sheet are uniformly distributed (refer to Fig. 1) to minimize the overall pressure drop in the packed columns. The indentations on the top edges of the coupon are a consequence of the preparation of the coupon sample from the metal sheets. Fig. 6(a) illustrates an instance of the extracted cross-sectional area profile at z = 12.6 mm, marked with red dots. The yellow and blue arrows represent the distribution of cross-sectional plane and surface normal vectors. The surface transition of the Mellapak coupons is relatively smooth, with no abrupt changes in the surface normal direction (see Fig. 5 and Fig. 6(a)). The perimeter, cross-sectional area, and width along the immersion direction of the reconstructed Mellapak coupon are displayed in Fig. 6(b-d). The reconstructed Mellapak coupon has a perimeter ranging from 41 mm to 48 mm (Fig. 6(b)). The fluctuation of the perimeter along the z direction is due to the wavy corrugated shape. The sharp drop in the perimeter around z = 10 mm is a result of the holes in the coupon geometry. A similar pattern is observed in the cross-sectional area profile of the coupons in Fig. 6(c). Conversely, the width of the coupon is relatively consistent from the bottom to the top edge, averaging 22.41 mm.

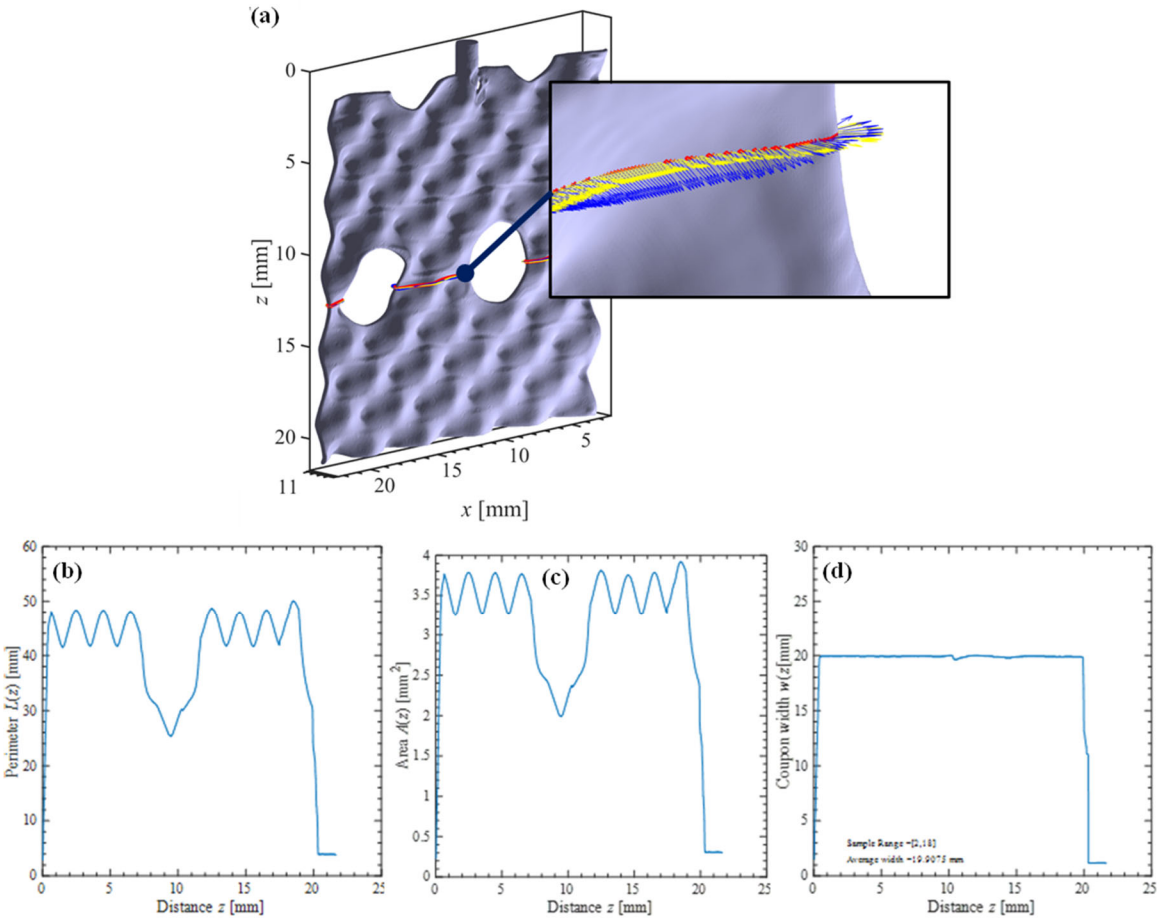

Fig. 6: (a) Visualization of the reconstructed 3D Mellapak coupon. (b) The perimeter, (c) cross-section area, and (d) width along the immersion direction (*z*.) of the reconstructed Mellapak coupon.

In addition, the flat SS coupon was fabricated with a regular geometry 20 mm (width) × 20 mm (length) × 0.29 mm (thickness). Therefore, its wetted perimeter (40.58 mm) is constant along the immersion depth.

3.0 Experiment Design and Description

The experimental setup was designed to investigate the effects of various factors such as packing surface structure, temperature, CO_2 loading, and surface movement (as a representative of contact line motion) on the contact angle measurement. The designed experiment was focused on evaluating Mellapak structures using aqueous solvent of 30% MEA by weight (30% MEA) at three temperatures. The experimental investigations were also designed to evaluate the operation of a CO_2 capture process on effective contact angle using the MEA solvent in a natural gas power plant.

Tensiometer force $F_t\ (z)$ is necessary to determine surface tension force $F_{\sigma,z}$ and the effective contact angle with a given solvent, as shown in Equation (1). Using a KRÜSS tensiometer K100C (KRÜSS GmbH, Hamburg, Germany), the surface tension and liquid density were assessed. As seen in Fig. 7(a), the tensiometer is connected to a recirculatory bath (NESLAB, Ex-111), a custom gas manifold, and a laptop computer for data acquisition. The temperature control jacket, which is plumbed to the recirculatory bath, was used to regulate the solvent's temperature (Fig. 7(b)). To regulate the gas environment and concentrations inside the sample chamber, the gas supply and vent lines are attached to the back of the tensiometer. CO_2 and nitrogen (N_2) gases are among the gases that are introduced into the system under the control of an externally plumbed manifold system.

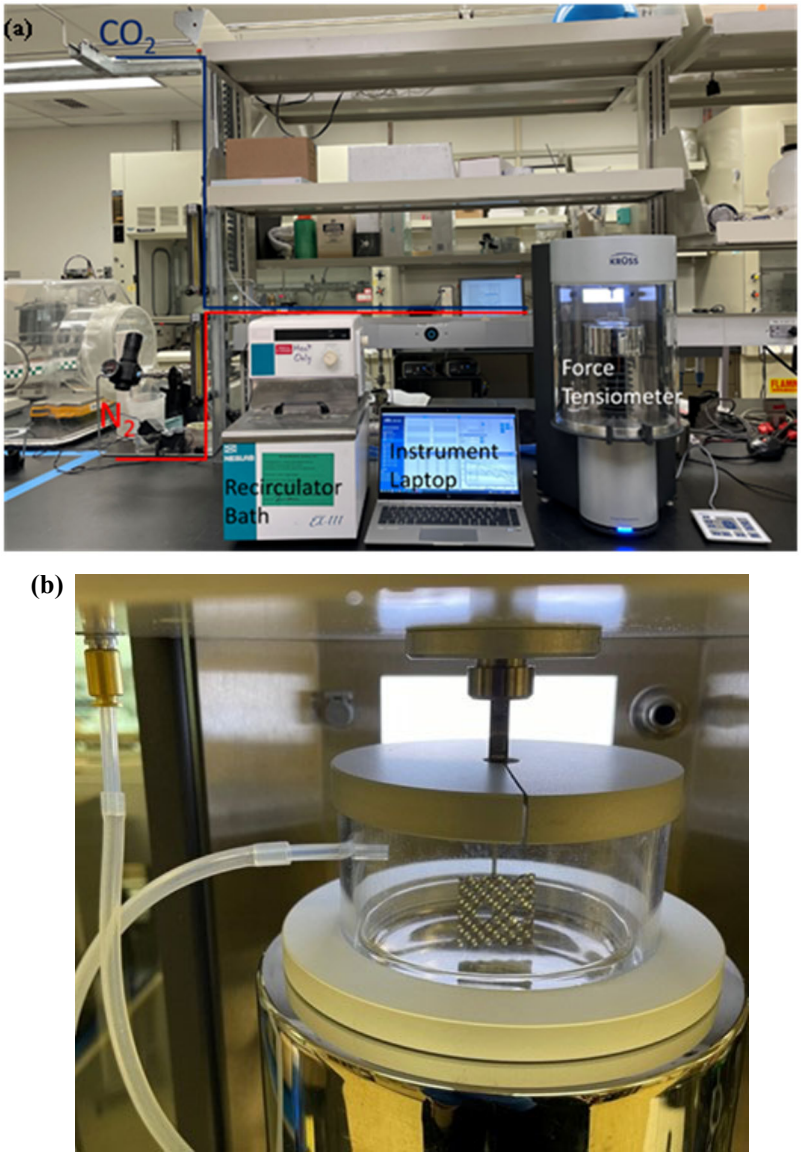

Fig. 7: (a) Photograph of the experimental setup including the KRÜSS K100C and its associated setup, a recirculatory bath, gas manifold, and instrument laptop. (b) Photograph of surface tension measurement using the Wilhelmy plate method with the gas flow through the gas enclosure

Before the surface tension measurement, the Wilhelmy plate was cleaned with organic solvent and deionized (DI) water subsequentially and heated to a red-hot temperature to burn off any impurities adhering to the surface. An amount of CO_2 that is known or desired is dissolved in the solvent using a specially built volumetric apparatus. The lean and rich solvent compositions estimated during continuous capture are used to determine these CO_2 loadings. To prepare the desired CO_2 loading for the respective MEA testing solutions, solid CO_2, also known as dry ice, was introduced. Initially, 100 g of the 30% MEA

solution was made by mixing 30 g MEA and 70 g DI water. The mixture was stirred using a magnetic stirrer bar within a glass vessel, employing the built-in stirring function of the force tensiometer. Subsequently, the dry ice pellets were incrementally added into the 30% MEA solution until the increased mass corresponded to the target CO_2 loading. It's important to note that most of the dry ice sublimated, and only the mass of the CO_2 that reacted with the solution was considered. The loaded solution was mixed by the stirrer bar and allowed to stand undisturbed for a period of 1 to 2 hours until it reached equilibrium.

The advanced software for operating the tensiometer was provided with instruments, which included modules for measuring surface tension using the Wilhelmy technique, liquid density, and dynamic contact angle, etc.

3.1 Surface tension measurement

In the Wilhelmy plate tests, the surface tension of testing solvents was necessary to compute the contact angles between the coupons and the solvent. A methodology for measuring the surface tension of various solvent with various CO_2 loadings has been developed. The solvents were poured into the glass vessel (shown in Fig. 7(b)) and placed within the force tensiometer's temperature control jacket. The gas enclosure was placed on top of the glass vessel, allowing gas to flow within. To aid in attaining temperature equilibrium, a magnetic stirrer bar was used to mix the test liquid. Methanol was used to clean the Wilhelmy plate, which was then washed with DI water. The Wilhelmy plate was then slowly cooled after being red heated on the micro burner. The surface tension template (SFT) offered by KRÜSS Advance software was used to measure the surface tension after inserting the Wilhelmy plate into the force tensiometer. Furthermore, the surface tension was measured before and after the determination of the contact angle, and the mean value of the surface tension was used in the calculation of the contact angle. Only advancing contact angles were used for analyses in this study.

3.2 Density measurement

Before and after the contact angle measurement, the density of the solvent was measured. Methanol was used to clean the standard measuring probe with a known density probe and probe holder, which is then ringed with DI water. The probe and probe holder were then blow- dried with N_2. The solvent density was measured using the liquid density determination template provided by the force tensiometer software.

The density probe holder was linked to the force sensor, and the force sensor was reset to zero. The density probe was then fitted to the probe holder and its weight was determined. The density probe was removed from the holder, and the liquid surface was detected by submerging the empty holder to calculate its contribution to the displacement. The total displacement was determined by immersing the density probe and holder in the solvent and measuring the density. After cleaning and drying the density probe and its holder, the density measurements were repeated.

3.3 Interfacial surface tension force measurement

Tensiometer force $F_\sigma\ (z)$ is required to calculate the effective contact angle for a given solvent and solid substrate, as shown in Equation (1). After measuring the surface tension and density of the solvent at the temperature and gas flow rate, the tensiometer force during immersion process was measured directly by the force tensiometer. Prior to the force measurement, the test coupon was cleaned with methanol, rinsed with DI water, and dried with N_2. The tensiometer force F_t is measured while the coupon's immersion depth (z) is increased and decreased. The tensiometer was linked to the coupon, and the gas enclosure was closed. The coupon was then prewetted for 120 seconds before being positioned around 2 mm above the liquid free surface. After connecting the coupon, the force sensor was reset to zero, and the liquid surface was detected to have a threshold value of 1. Following that, the tensiometer force was measured with an immersion and receding speed of 1 mm/min. As previously stated, the immersion depth was set at 12 mm with a position step of 0.1 mm. The tensiometer force was measured in relation to the sample's location during immersion and withdrawal.

3.4 Solvent and materials

Next using fabricated coupon wafers from structured packing materials (Sulzer Mellapak) that have surface geometries similar to those of the column packing materials, contact angle measurements can be performed. As a control, flat coupon wafers made from 316 SS (material of construction for Mellapak packing) were also fabricated to evaluate and deconvolute the impact of material composition and surface features on the contact angle and wetting.

To systematically control wetting properties on a given surface, a solvent of NaOH was used as the solvent surrogate. This solvent can be tuned with varying amounts of surfactant additives to increase the surface tension and consequently the contact angle upon wetting the packing surface. To perform these measurements on the tensiometer, an aqueous 0.10 M NaOH stock solvent was prepared, and aliquots of this solvent were varied containing precisely measured parts per million (ppm) concentrations of Tergitol NP-7 surfactant. The Wilhelmy plate measurements that yielded the evaluated surface tension at 30 °C for these varying solvents are summarized in Table 1 and plotted in Fig. 8. The experimental data collected from the Wilhelmy plate experiments are shown to be reproducible given the consistency of repeat runs in measuring the same surface tension.

Table 1. Testing solvents of 0.1M NaOH mixed with varying concentration levels of surfactant and the resulting surface tension measured at 30 °C.

Surfactant (ppm)	Surface Tension (mN/m)
0	71.50
0.5	59.21
1	51.87
2	47.71
5	42.57
10	40.08
20	34.08
30	29.97
40	30.07

The surface tension data for the varying NaOH solvents were correlated to an empirical dual exponential decay function with the fit shown in Fig. 8. As shown by the data and the fit, very small concentrations of

surfactant have a significant impact on surface tension and this impact is lessened as the concentration increases. For the range of 0–40 ppm surfactant added, the surface tension of the NaOH solvent is observed to decrease from 72 to ~30 mN/m. To independently check the correlation obtained, additional spot check experiments at other surfactant concentrations (0.5 ppm and 2 ppm) were also performed. The measured values were 59.21 and 47.21 mN/m, respectively. The calculated surface tension for these two solvents, according to the generated correlation equation (Fig. 8), are 58.27 and 46.86 mN/m accordingly.

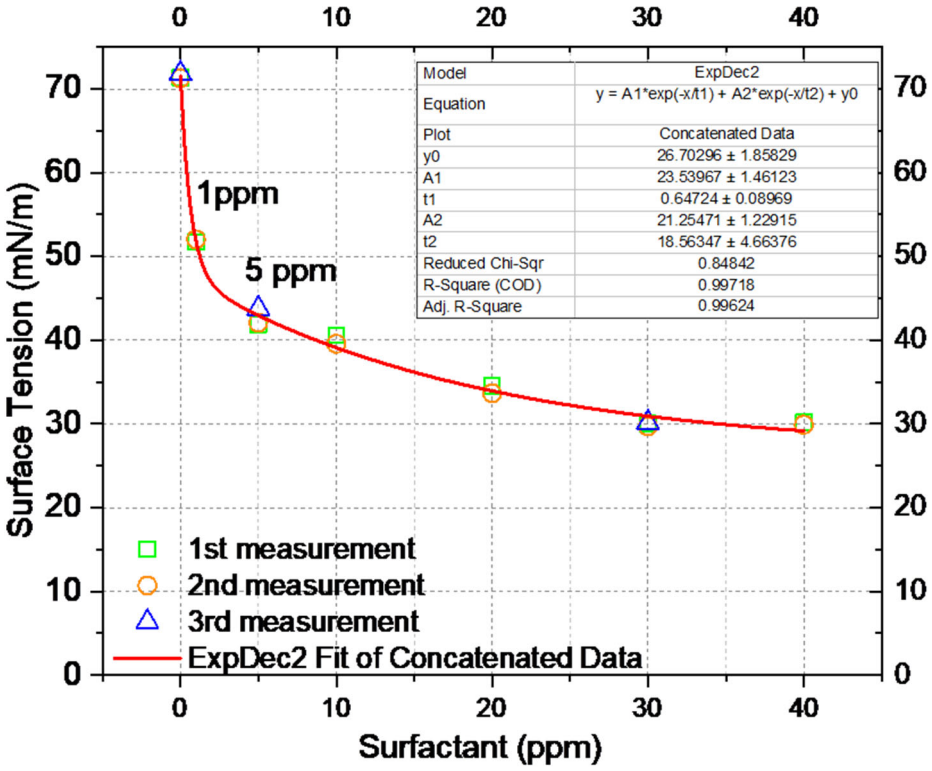

Fig. 8: Surface tension vs. surfactant concentration (including curve fitting) for varying antifoam solvents of 0.10M aqueous NaOH solvent tested on the tensiometer at 30 °C.

In addition to the impact of surfactant in aqueous NaOH solvent, the presence of a foam mitigator (antifoam) is necessary to prevent foam accumulation during column tests involving countercurrent gas/solvent flow in the absorber. Using a high concentration of surfactant (30 ppm) and a fixed representative concentration of antifoam/defoamer (50 ppm), standard foam tests (ASTM D6082 − 12 (2017)) were performed using a sparger and bubbling gas into a graduated cylinder containing the solvent mixture. As observed in the photographs shown in Fig. 9, the defoamer—TRANS 713 petroleum

distillate—showed significant mitigation of foam compared to the antifoam analog. The surface tensions of the solvents containing both surfactant and antifoam/defoamer were also verified to follow the correlation established with surfactant-only surface tension experiments (Table 2). Based on these results, future column experiments with NaOH solvents will use a controlled amount of surfactant in addition to 50 ppm defoamer. Note that the impact of both surfactant and defoamer on the quantity and rate of CO_2 solubility in NaOH has not yet been verified.

Table 2. The volume of foam at 5 minutes of N_2 purging and at 1 minute after purging stopped.

Chemical	@ 5 min of N_2 Purging		@ 1 min after N_2 Purging	Surface Tension (mN/m)
	Static Foam (mL)	Dynamic Foam (mL)	Static Foam (mL)	
antifoam	50-55	20-30	10-20	30.03
defoamer	<5	10-15	<1	30.77

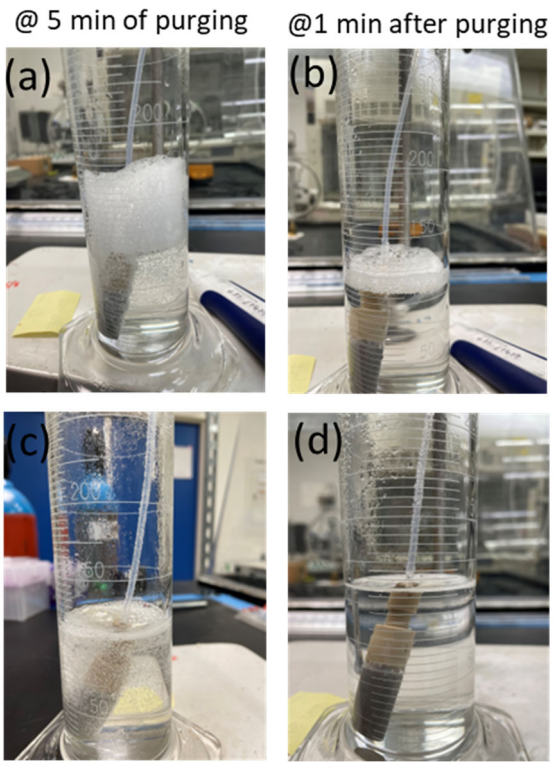

Fig. 9: Photographs of foam testing of NaOH solvents via sparger and the effect of preventing foam formation (50 ppm antifoam (a-b) vs. 50 ppm defoamer (c-d)).

3.5 Solvent properties at various CO_2 loadings

To dissolve a known/desired amount of CO_2 in the solvent, dry ice was used as the CO_2 source. The CO_2 loadings were determined by estimating the lean and rich solvent compositions during continuous capture. A desired water composition is introduced to this solvent by mass. The initial solvent vapor pressure is ignored for the CO_2 loading computation due to the low vapor pressure of the aqueous 30% MEA solvent. Variation of the surface tension with temperature is presented in Fig. 10 for different CO_2 loadings. The surface tension value decreases with the increased value of the temperature under all CO_2 loading conditions.

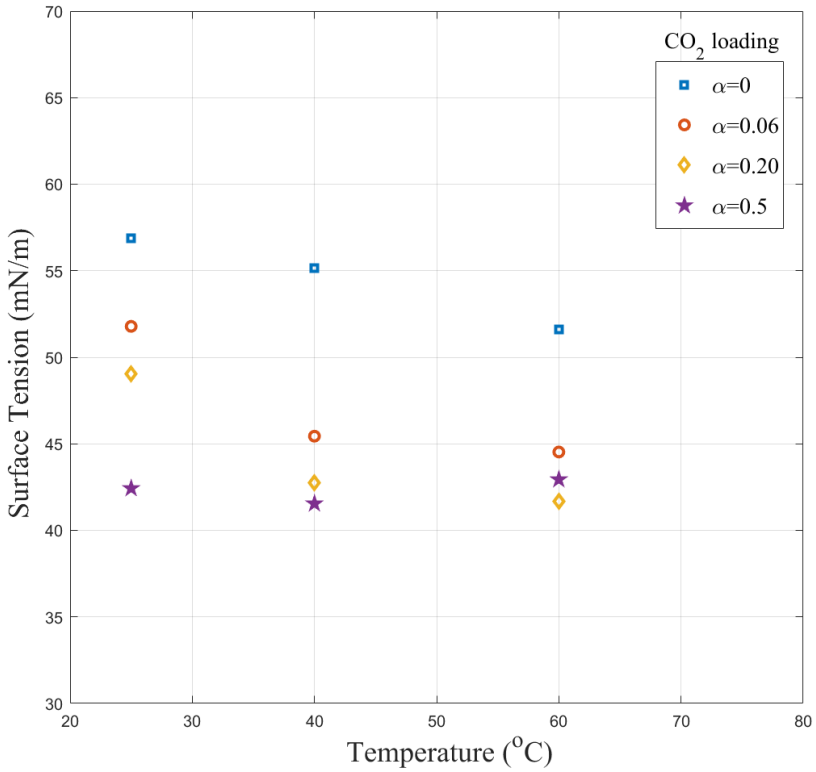

Fig. 10: Variation of the surface tension of the aqueous 30% MEA solvent at different temperatures and CO_2 loadings (α).

4.0 Results and Discussion

The control of wetting behavior via solvent composition modification was probed by conducting dynamic contact angle measurements of the tensiometer using the pre-determined surface tension correlation. The surfaces tested for contact angle measurements included the Mellapak sheet and a flat, smooth SS surface. Contact angle measurements were performed by immersing and retracting the coupon wafers in and out of the NaOH solvents at a known speed. The wetting length of the coupon wafers was computed from their corresponding 3D-XCT scanned images. Based on the design of the coupon model, solvent property and tensiometer force data, the effective contact angle for a given pair of packing coupon and solvent were calculated. The contact angle for flat stainless steel sheet was used for verification of the present methodology. This the effective contact angle measurement for the flat blank sheet and Mellapak coupons is discussed below.

4.1 Effective contact angle for the flat stainless coupon

The flat blank coupon here is used as an example to show the verification of the experimental method for effective contact angle measurement. The surface tension force $F_{\sigma,z}$ is calculated by accounting for the buoyancy force. In this study, the plate was set to move at a low velocity of 1 mm/min to avoid higher contact line motion. In this view, advancing and receding force data are nearly the same across all the immersion positions at this speed. This suggests that the final advancing and receding contact angles would be close, and the contact angle hysteresis would be insignificant given the low contact line moving velocity for the flat blank coupon. Because all the experiments are carried at the 1 mm/min immersion speed, only the advancing force curve would be selected for the effective contact angle calculation for all the tested coupons. Under ideal conditions, the surface tension force curve for a standard Wilhelmy plate should be flat after the buoyancy force correction. Multiple factors can cause the deviations in the value of contact angle. A more detailed investigation would be necessary to understand the sources of uncertainty affecting the measurement of surface tension and buoyancy force corrections. Fig. 11 shows the variation of the effective contact angle with the surface tension value for flat blank coupons as well as for Mellapak

coupons. Note that the carbon capture is carried out with prewetted coupons. Accordingly, both coupons were prewetted before immersion of the coupons in the test solvents. In this case. two solvents, namely DI water and 0.1M aqueous NaOH solvents, were chosen for the test. As explained earlier, the surface tension of the DI water was altered using surfactant and defoamer. The effective contact angle increased with the increased surface tension value, which was somewhat expected. Next, the value of the effective contact angle of the aqueous 0.10 M NaOH solvent for the prewetted plate showed the higher values. Note that the 0.10 M NaOH aqueous solvent had the highest value of surface tension among the solvents studied. A solvent with higher surface tension values shows higher values of the contact angle for a flat and homogenous sheet [31]. Further, the measured value of the contact angle matched well with the corresponding value available in the open literature [5]. Therefore, reasonable matching with the experimental value verified the present methodology of contact angle measurement, and experiments were further conducted for measuring the contact angle for Mellapak packing.

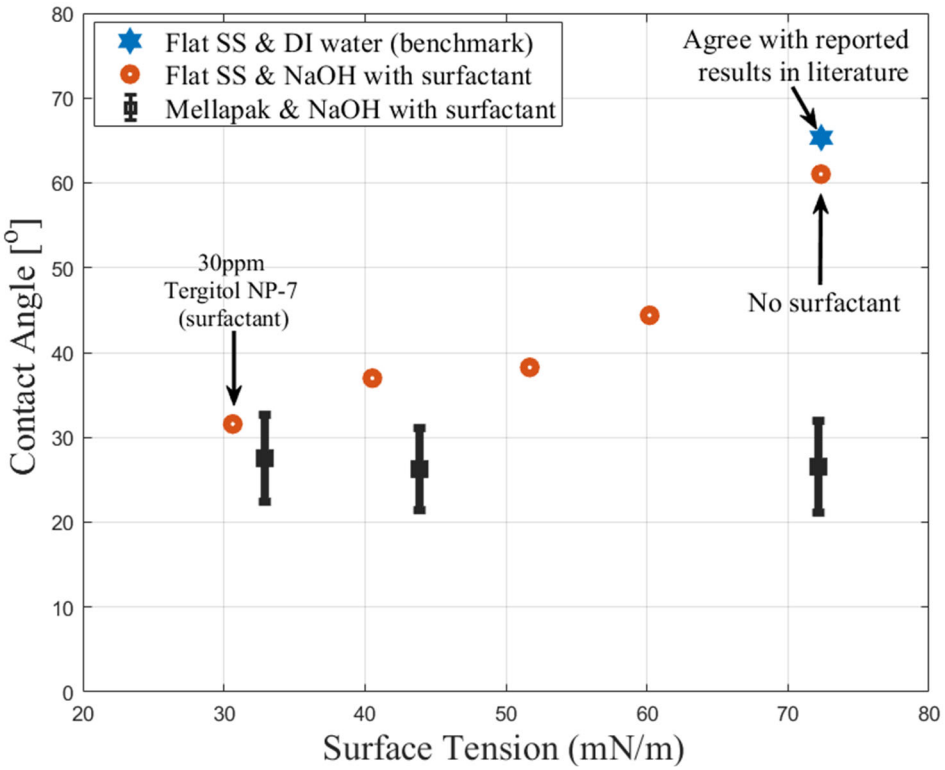

Fig. 11: Variation of the contact angle with the surface tension for flat blank SS and Mellapak coupons with different solvents at 30 °C.

4.2 Effective contact angle for the Mellapak coupon

As mentioned previously, the value of the surface tension of the 0.10 M aqueous NaOH solvent was changed with surfactant. In this condition, the Mellapak coupon was tested at the temperature of 30 ºC. As can be seen in Fig. 11, the value of effective contact does not change with the changing value of the surface tension of the aqueous NaOH solvent. As seen in Fig. 11, a flat smooth coupon shows the increased value of contact angles with the increasing value of surface tension for the same solvent. The approximately constant value of the effective contact angle is due to surface texture and the design of Mellapak sheet. The curve period is around 2 mm, which reflects the coupon surface feature wavelength. This corresponds to the location where the contact line starts to pass through the two perforated holes on the packing coupon surface. The reduced wetting length results in a smaller surface tension force.

Next, three representative solvents containing varying concentrations of surfactant were tested on the Mellapak coupon (Fig. 12). As observed from the data, the prewetted coupon showed little impact on contact angle regardless of solvent surface tension. This was counterintuitive to literature (Fig. 4a) that reported that static contact angle measurements (performed on a goniometer) were performed on smooth, flat surfaces of corresponding material and were shown to have a direct correlation with surface tension. As noted, the difference between the literature experiments was (1) the lack of surface features/textures tested' (2) the dry starting condition of the surface, and (3) the contact angle measurement methodology (static vs dynamic). The same experiments were repeated, this time without prewetting the coupon, and the observed data did show some impact as a function of surface tension, although it was minimal. It is deduced from these data that the surface features/textures play a prominent role in dampening the contribution of surface tension to the wetting behavior. To verify this uniquely observed behavior, control tests were performed in the same protocol with a smooth, flat coupon of the same material composition without any surface features/textures. The data obtained from these experiments (Fig. 11) confirmed behavior as expected; higher surface tension solvents showed larger contact angles and reduced wetting compared to lower surface tension solvents. This corroborates the assumption that the surface features/textures of

representative column packing material Mellapak 500.Y are observed to show no impact on contact angle as a function of surface tension. However, this does not imply that surface tension will not affect wetting behavior in column packing. This must be ultimately verified with packed column tests. Future tensiometer experiments will also verify this impact of surface features on surfaces made of another materials using coupon wafers composed of plastic/polymer resin instead of steel. Ultimately, after NaOH surrogate solvent testing, these wetting behavior findings can be translated to prospective solvent candidate CO_2 capture solvents, 2-EEMPA.

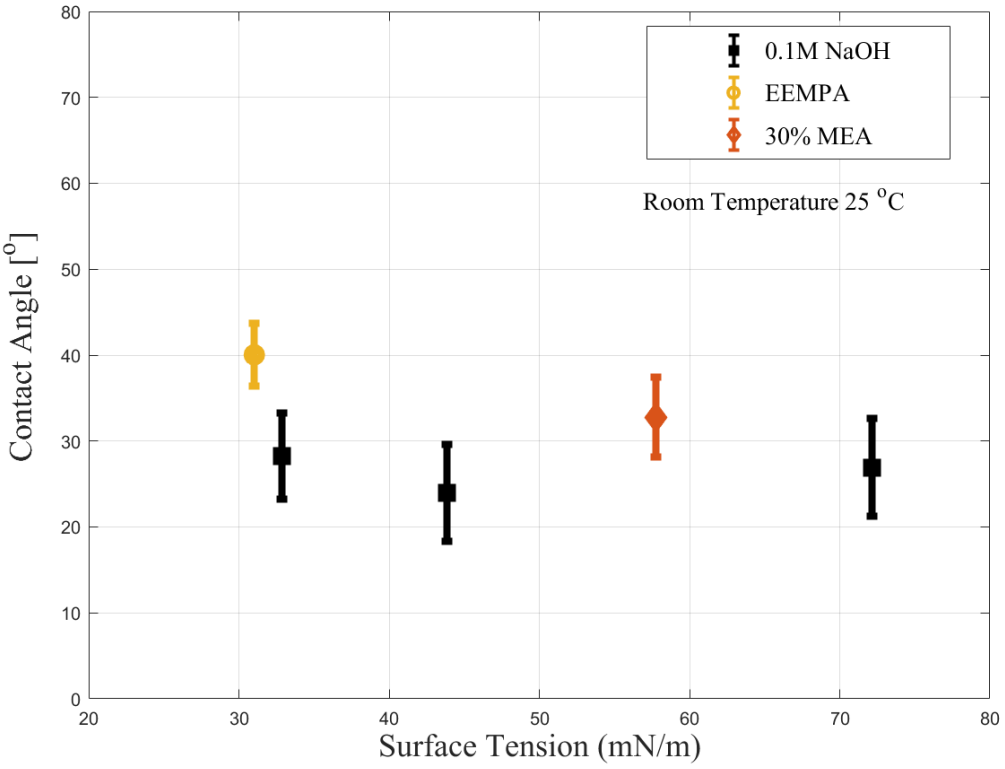

Fig. 12: Effective contact angle distribution for the Mellapak coupon at 25 °C for different solvents.

4.3 Effect of temperature on contact angle

The corrected surface tension force $\hat{F}_{\sigma,z}$ profiles for the Mellapak without coating were calculated first and contact angles were calculated using the intersection method. Note that a packed column can work at different temperatures depending on the inlet flue gas temperature. Indeed, temperature varies axially across the height of column. Because solvent properties vary with temperature, variation in the contact angle is

expected. Accordingly, the contact angle of the aqueous 30% MEA solvent for the Mellapak coupon was examined at three temperatures (25 ºC, 40 ºC, and 60 ºC). In addition, aqueous 0.1M NaOH solvent at 25°C and different surfactant concentrations was also tested. In Fig. 13, it can be observed that the contact angle does not change significantly under all conditions; there is only slight variation in the contact angles. This further confirms that surface texture, embossment and holes in the sheet play key roles in the contact angle measurement.

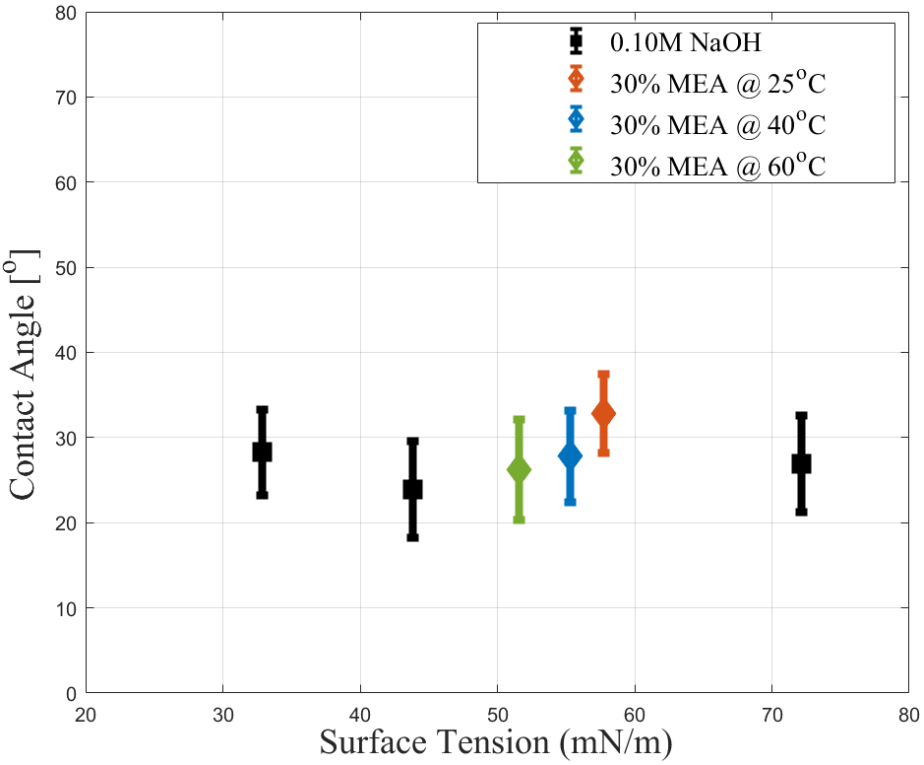

Fig. 13: Effective contact angle distribution for the Mellapak coupon using aqueous 0.10 M NaOH and 30% MEA solvents at different temperatures.

4.4 Effect of the CO_2 loadings on the contact angle

Similar to temperature variation, CO_2 loading in the solvents also varies throughout the packed column. Solvent at the bottom of the packed column has enriched CO_2 loading, while the top of the column may have lean solvent. In addition, 30% MEA shows different CO_2 loading conditions at coal-fired and natural gas plants for CO_2 capture conditions. Accordingly, the effect of the CO_2 loadings on the contact angles for Mellapak coupons and aqueous 30% MEA solvent were studied at a fixed temperature of 25°C. Next, the

value of the effective contact angle was compared with pure 30% MEA solvent. Fig. 14 shows the variation of the effective contact angles with CO_2 loading for Mellapak coupons. With increased CO_2 loading, the effective contact angle becomes larger compared to that with the pure 30% MEA solvent at different temperatures. The different values of surface tension at a given CO_2 loading were achieved by varying temperature of a solvent. Note the surface tension of solvents decreases with increased temperature [32]. An increase in CO_2 loading can decrease the effective contact angle for the CO_2-loaded aqueous 30% MEA solvent (see Fig. 14).

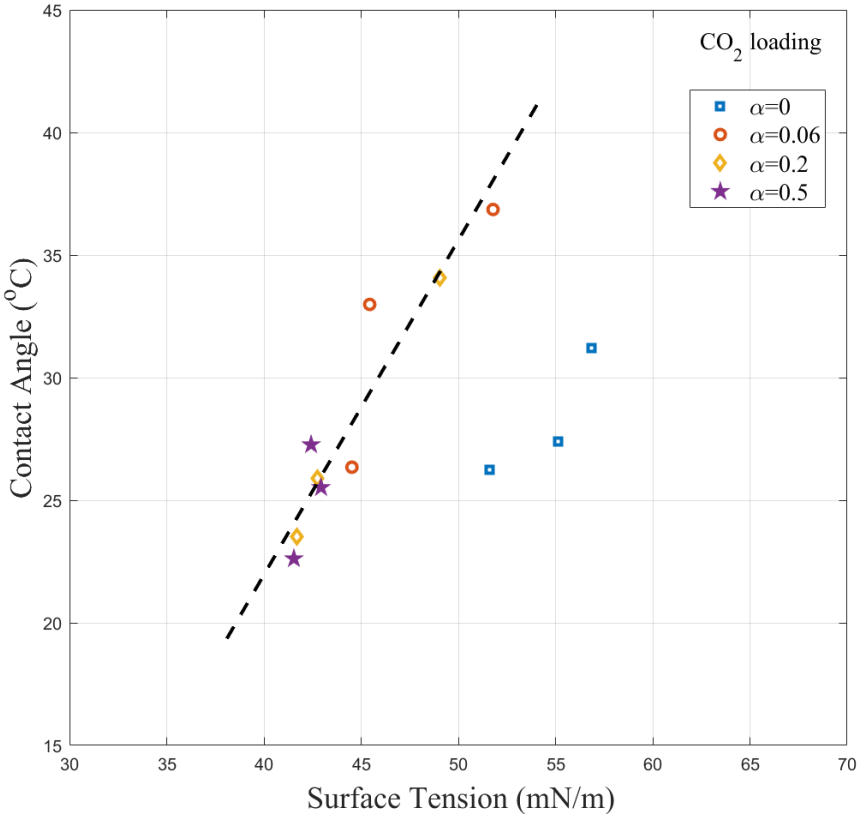

Fig. 14: Effective contact angle distribution for the Mellapak coupon at different CO_2 loadings and temperatures.

5.0 Conclusion

The interaction of the packing surface with the solvent is important in the wetting process of packings and therefore the effective mass transfer area in the packed column used in the absorption process. Using the Wilhelmy plate method, an efficient contact angle measuring methodology has been developed. The current methodology considers the packing surface characteristics (texture, embossment, and perforated holes) as well as the solvent property. The suggested methodology, when compared to the optical approach and the classic Wilhelmy plate method, provides a more accurate determination of the effective contact angle and minimizes measurement uncertainty for a given pair of solvent and packing coupon. At various CO_2 loadings and temperatures, the contact angles for aqueous solvents (0.10 M NaOH and 30% MEA) were acquired, and the water-lean carbon capture solvent, EEMPA, was also explored.

The effective contact angle for the flat sheet and Mellapak coupons was examined for different solvents. Experiments were conducted for stainless steel coupons using DI water and aqueous 0.10M NaOH solvent for verification purpose. The effective contact angle increased with the increased value of the surface tension for flat SS sheet. On the other hand, the effective contact angles did not vary in Mellapak coupons for aqueous MEA and NaOH solvents. In this case, surface textures and sheet design played a dominant role over the surface tension of solvents. Furthermore, CO_2 loading had a significant effect on the contact angle for Mellapak coupons. As expected, contact angle decreased with the increasing temperature of CO_2 capture solvents (MEA, EEMPA).

The effective contact angle measurement using the Wilhelmy plate method provided more accurate and efficient solvents for characterizing the solvent-packing surface interactions. Subsequently, it enhanced the accuracy in the prediction of interfacial area in carbon capture by solvent absorption. Further, its use will significantly benefit the development of new solvents and the design of new packings for CCSs. The effective contact angle for a wide range of solvent and packing coupon pairings may be measured easily using the newly defined procedure. It can also improve the understanding of the effective mass transfer area of a gas-liquid contacting system, which will lead to a benefit for solvent systems throughout the entire CO_2

collection program. With a narrow distribution range of contact angle, the accuracy of the effective mass transfer area prediction would be enhanced by integrating the experimental data of contact angle in the computational fluid dynamics to develop surrogate process model.

Reference

1. Razi, N., O. Bolland, and H. Svendsen, *Review of design correlations for CO2 absorption into MEA using structured packings.* International Journal of Greenhouse Gas Control, 2012. **9**(0): p. 193-219.
2. Spiegel, L. and W. Meier, *Distillation Columns with Structured Packings in the Next Decade.* Chemical Engineering Research and Design, 2003. **81**(1): p. 39-47.
3. Jiang, Y., et al., *Techno-economic comparison of various process configurations for post-combustion carbon capture using a single-component water-lean solvent.* International Journal of Greenhouse Gas Control, 2021. **106**: p. 103279.
4. Mackowiak, J., *Fluid Dynamics of Packed Columns*. 2010, Berlin: Springer-Verlag.
5. Tsai, R.E., *Mass Transfer Area of Structured Packing*, in *Chemical Engineering*. 2010, The University of Texas at Austin: Austin, TX. p. 400.
6. Tsai, R.E., et al., *Influence of Surface Tension on Effective Packing Area.* Industrial & Engineering Chemistry Research, 2008. **47**(4): p. 1253-1260.
7. Tsai, R.E., et al., *Influence of viscosity and surface tension on the effective mass transfer area of structured packing.* Energy Procedia, 2009. **1**(1): p. 1197-1204.
8. Tsai, R.E., et al., *A dimensionless model for predicting the mass-transfer area of structured packing.* AIChE Journal, 2011. **57**(5): p. 1173-1184.
9. Shi, M.G. and A. Mersmann, *Effective interfacial area in packed columns.* German chemical engineering, 1985. **8**(2): p. 87-96.
10. Singh, R.K., et al., *Hydrodynamics of countercurrent flow in an additive manufactured column with triply periodic minimal surfaces for carbon dioxide capture.* Chemical Engineering Journal, 2022.
11. Singh, R.K., J.E. Galvin, and X. Sun, *Three-dimensional simulation of rivulet and film flows over an inclined plate: Effects of solvent properties and contact angle.* Chemical Engineering Science, 2016. **142**: p. 244-257.
12. Singh, R.K., J.E. Galvin, and X. Sun, *Hydrodynamics of the rivulet flow over corrugated sheet used in structured packings.* International Journal of Greenhouse Gas Control, 2017. **64**: p. 87-98.
13. Singh, R.K., J.E. Galvin, and X. Sun, *Multiphase flow studies for microscale hydrodynamics in the structured packed column.* Chemical Engineering Journal, 2018. **353**: p. 949-963.
14. Rocha, J.A., J.L. Bravo, and J.R. Fair, *Distillation columns containing structured packings: a comprehensive model for their performance. 1. Hydraulic models.* Industrial & Engineering Chemistry Research, 1993. **32**(4): p. 641-651.
15. Zeng, C., et al., *Differentiation of static and dynamic interfacial area in the structured packed column.* Chemical Engineering Science, 2022. **260**.
16. Fu, Y., et al., *The influence of random packed column parameters on the liquid holdup and interfacial area.* AIChE Journal, 2022.
17. Singh, R.K., et al., *Hydrodynamics of countercurrent flows in a structured packed column: Effects of initial wetting and dynamic contact angle.* Chemical Engineering Journal, 2020. **398**.
18. Fourati, M., V. Roig, and L. Raynal, *Experimental study of liquid spreading in structured packings.* Chemical Engineering Science, 2012. **80**: p. 1-15.
19. Snoeijer, J.H. and B. Andreotti, *A microscopic view on contact angle selection.* Physics of Fluids, 2008. **20**(5): p. 057101.
20. Kohrt, M., et al., *Texture influence on liquid-side mass transfer.* Chemical Engineering Research and Design, 2011. **89**(8): p. 1405-1413.
21. Wenzel, R.N., *Resistance of solid surfaces to wetting by water.* Industrial & Engineering Chemistry, 1936. **28**(8): p. 988-994.

22. Nicolaiewsky, E.M.A. and J.R. Fair, *Liquid Flow over Textured Surfaces. 1. Contact Angles.* Industrial & Engineering Chemistry Research, 1998. **38**(1): p. 284-291.
23. Billet, R. and M. Schultes, *Prediction of Mass Transfer Columns with Dumped and Arranged Packings.* Chemical Engineering Research and Design, 1999. **77**(6): p. 498-504.
24. Gualito, J.J., et al., *Design Method for Distillation Columns Filled with Metallic, Ceramic, or Plastic Structured Packings.* Industrial & Engineering Chemistry Research, 1997. **36**(5): p. 1747-1757.
25. Chau, T.T., et al., *A review of factors that affect contact angle and implications for flotation practice.* Adv Colloid Interface Sci, 2009. **150**(2): p. 106-15.
26. Sebastia-Saez, D., S. Gu, and M. Ramaioli, *Effect of the contact angle on the morphology, residence time distribution and mass transfer into liquid rivulets: A CFD study.* Chemical Engineering Science, 2018. **176**: p. 356-366.
27. Wilhelmy, L., *Ueber die Abhängigkeit der Capillaritäts-Constanten des Alkohols von Substanz und Gestalt des benetzten festen Körpers.* Annalen der Physik, 1863. **195**(6): p. 177-217.
28. Zheng, R.F., et al., *A single-component water-lean post-combustion CO2 capture solvent with exceptionally low operational heat and total costs of capture – comprehensive experimental and theoretical evaluation.* Energy & Environmental Science, 2020. **13**(11): p. 4106-4113.
29. Heldebrant, D.J., et al., *Are Water-lean Solvent Systems Viable for Post-Combustion CO2 Capture?* Energy Procedia, 2017. **114**: p. 756-763.
30. Fu, Y., et al., *Determination of effective contact angle for CO2 capture column packing coupons with Wilhelmy plate experiments.* . 2021, Pacific Northwest National Laboratory: United States. p. 1 - 33.
31. Zisman, W.A., *Relation of the Equilibrium Contact Angle to Liquid and Solid Constitution*, in *Contact Angle, Wettability, and Adhesion*. 1964, American Chemical Society. p. 1-51.
32. Idris, Z., et al., *Surface Tension of Alkanolamine Solutions: An Experimentally Based Review.* Energy Procedia, 2017. **114**: p. 1828-1833.